Development 130, 753-762

doi:10.1242/dev.00290

Three Brick genes have distinct functions in a common pathway promoting polarized cell division and cell morphogenesis in the maize leaf epidermis

Mary J. Frank, Heather N. Cartwright and Laurie G. Smith

Section of Cell and Developmental Biology, U.C. San Diego, 9500 Gilman Drive, La Jolla, CA 92093-0116, USA
*Author for correspondence (e-mail: lsmith@biomail.ucsd.edu)

Accepted 29 October 2002

SUMMARY

We have taken a genetic approach to investigating cytoskeleton-dependent mechanisms governing cell morphogenesis in the maize leaf epidermis. Previously, we showed that the *Brick1* (*Brk1*) gene is required for the formation of epidermal cell lobes as well as for properly polarized divisions of stomatal subsidiary mother cells, and encodes an 8 kDa protein highly conserved in plants and animals. Here, we show that two additional Brick genes, *Brk2* and *Brk3*, are involved in the same aspects of epidermal cell morphogenesis and division. As shown previously for *Brk1*, analysis of the cytoskeleton shows that *Brk2* and *Brk3* are required for the formation of local F-actin enrichments associated with lobe outgrowth in wild-type cells. Analysis of *brk1;brk2*, *brk1;brk3* and *brk2;brk3* double mutants shows that their phenotypes are the same as those of *brk* single mutants. Mosaic analysis shows that *Brk1* acts non cell-autonomously over a short distance. By contrast, *Brk2* and *Brk3* act cell-autonomously to promote pavement cell lobe formation, but *Brk3* acts non cell-autonomously, and *Brk2* partially non cell-autonomously, to promote polarized subsidiary mother cell divisions. Together, these observations indicate that all three *Brk* genes act in a common pathway in which each *Brk* gene has a distinct function. Recent work demonstrating a function for the mammalian homolog of BRK1 (HSPC300) in activation of Arp2/3-dependent actin polymerization implicates the *Brk* pathway in local regulation of actin polymerization in plant cells.

Key words: Cell polarity, Cell morphogenesis, Maize leaf development, Mosaic analysis, BRICK1, HSPC300

INTRODUCTION

Plant cells' shapes are defined by their surrounding walls. Consequently, cell shapes are determined by patterns of wall expansion during organ growth. Most plant cells expand by means of anisotropic, diffuse growth, with expansion distributed across the cell surface but oriented preferentially in one or more directions. A few highly elongated cell types such as pollen tubes and root hairs expand by means of tip growth, an extremely polarized mode of cell expansion in which growth is focused at a single site on the cell surface. The mechanisms underlying these different modes of cell expansion remain to be fully elucidated but both depend critically on the cytoskeleton.

Drug studies have demonstrated crucial roles for F-actin in tip growth, one of which is to transport secretory vesicles containing cell wall components along longitudinal F-actin bundles to the vicinity of the growth site (Geitmann and Emons, 2000; Hepler et al., 2001). A fine meshwork of cortical F-actin observed at or near the growth site in tip growing cells is thought to have a function separate from that of the longitudinal F-actin bundles, which is not well understood (Geitmann and Emons, 2000; Hepler et al., 2001). Pharmacological and genetic studies have shown that F-actin also promotes the expansion of diffusely growing cells (Smith, 2003). By analogy to its well-established role in tip growth, it has been proposed that the primary role of F-actin in diffusely growing cells is to guide the deposition of secreted wall components (Baskin and Bivens, 1995; Dong et al., 2001).

As the principal structural component of the primary cell wall, cellulose is thought to constrain cell expansion and thereby function as a key determinant of shape in diffusely growing cells. Drug studies have shown that normal patterns of diffuse growth also depend on microtubules, which, during interphase, are arranged in the cell cortex in a pattern mirroring that of cellulose deposition into the wall (Cyr, 1994). Although the precise nature of the relationship linking microtubule organization to cellulose deposition pattern remains unknown, it has been proposed that microtubules help to guide the deposition pattern of cellulose microfibrils into the wall (Giddings and Staehelin, 1991; Baskin, 2001).

Some plant cells acquire complex shapes through multidirectional cell expansion patterns involving both microtubule and actin-dependent mechanisms. Three-branched trichomes that form on the *Arabidopsis* epidermis provide a good example. Drug studies have established that microtubules, but not actin filaments, play a crucial role in the initial polarized outgrowth of trichomes and trichome

branches. However, subsequent outgrowth of trichome branches proceeds by means of an actin-dependent, diffuse growth process (Szymanski et al., 1999; Mathur et al., 1999) (M. Hülskamp, personal communication). Mutations disrupting various aspects of trichome morphogenesis have identified dozens of genes required for the proper shaping of this cell type (Bouyer et al., 2001). Molecular analysis of some of the corresponding genes has begun to shed light on microtubule-dependent mechanisms involved in branch formation (Oppenheimer et al., 1997; Burk et al., 2001; Folkers et al., 2002; Kim et al., 2002). Further molecular analysis of these and other gene products yet to be identified will undoubtedly advance our understanding of both microtubule- and F-actin-dependent mechanisms governing trichome morphogenesis.

The lobed shapes of leaf epidermal and mesophyll cells provide another example of a complex shape resulting from multidirectional cell expansion. Lobes arise as polarized outgrowths at multiple sites along the margins of cells whose overall size is increasing via diffuse growth. In lobe-forming cells from a wide variety of species, emergence of lobes is associated with reorganization of cortical microtubules into bands focused at lobe sinuses (Jung and Wernicke, 1990; Apostolakos et al., 1991; Wernicke et al., 1993; Panteris et al., 1993a; Panteris et al., 1993b; Panteris et al., 1994; Wasteneys et al., 1997; Qiu et al., 2002; Frank and Smith, 2002). Microtubule bands have been proposed to direct the localized deposition of cellulose, creating periodic wall thickenings; intervening thinner regions of the wall are presumed to be more extensible, bulging out under the force of turgor pressure to form lobes.

Far fewer studies have considered the role of F-actin in lobe formation. In expanding wheat mesophyll cells, bands of cortical F-actin were observed to co-localize with microtubule bands; cytochalasin treatments suggested an important role for F-actin in the organization of cortical microtubule bands (Wernicke and Jung, 1992). However, two recent studies have provided evidence of a different role for F-actin in the formation of epidermal cell lobes. These studies showed that, in expanding epidermal cells of maize and *Arabidopsis*, localized enrichment of cortical F-actin is observed at the tips of emerging lobes, somewhat similar to the F-actin arrangement at the tips of tip-growing cells (Frank and Smith, 2002; Fu et al., 2002). Expression of dominant negative and constitutively active forms of ROP2 (a Rho-related GTPase) disrupted the formation or localization of these cortical F-actin enrichments and also perturbed the formation of lobes (Fu et al., 2002). In maize *brk1* mutants, epidermal lobes completely fail to form, although cells expand to achieve a normal overall size. Loss of lobes on *brk1* mutant epidermal cells is associated with a failure of localized cortical F-actin enrichments to form, whereas cortical microtubules bands are still present (Frank and Smith, 2002). Thus, both studies suggest a crucial role for localized F-actin enrichments in epidermal lobe formation separate from simply promoting the formation of microtubule bands.

In addition to its effects on epidermal pavement cell shape, *brk1* causes 20-40% of stomatal subsidiary cells to form abnormally (Gallagher and Smith, 2000). In wild-type leaves, subsidiary cells arise from the asymmetric divisions of subsidiary mother cells (SMCs), whose premitotic polarization involves the formation of a localized enrichment of F-actin at a specific site in the cell cortex. Interestingly, abnormal *brk1* subsidiary cells could be attributed to defects in the polarization of SMCs associated with loss of this localized enrichment of cortical F-actin (Gallagher and Smith, 2000). Thus, our observations have revealed a mechanistic link between the formation of polarized outgrowths on the margins of expanding epidermal cells and the polarization of premitotic SMCs, and suggest a role for *Brk1* in an actin-dependent aspect of both processes.

In this study, we present an analysis of two additional mutants, *brk2* and *brk3*, which have essentially the same phenotype as *brk1*. Through a combination of phenotypic, double mutant and mosaic analyses, we demonstrate that all three *Brk* genes have distinct functions in a common pathway promoting lobe formation and polarized cell division in the maize leaf epidermis.

MATERIALS AND METHODS

Isolation, allelism testing and mapping of *brk* mutations

Leaves from EMS-mutagenized lines of maize (a generous gift from L. Harper and M. Freeling, UC Berkeley) were screened by making impressions of the leaf surface in Loctite cyanoacrylate glue and examining them in a stereomicroscope for altered epidermal cell shapes. Nine independent mutations with a *brk1*-like phenotype were identified, which were found to define two new complementation groups, *brk2* (with five alleles) and *brk3* (with four alleles). At least two sequential crosses into the B73 inbred background were carried out prior to use of mutants for phenotypic analysis or for crosses to generate double mutants.

The *brk2* and *brk3* mutations were mapped to chromosome arms using B-A translocations (Beckett, 1994). The *brk2* locus is located on chromosome arm 1S, and *brk3* on 10S. Linkage analysis with visible genetic markers on 1S showed that *brk2* is ~6 cM from *Vp5*. More precise mapping relative to restriction fragment length polymorphism markers showed that *brk2* is ~7 cM from *asg31* at the distal end of 1S, and *brk3* is less than 4 cM from *php20075a* near the tip of 10S.

Analysis of *brk* phenotypes

Epidermal peels were prepared and stained with Toluidine Blue O as described by Gallagher and Smith (Gallagher and Smith, 1999). For cross sections, mature adult leaf pieces were fixed in 4% formaldehyde/50 mM KPO_4 pH 7 for at least 2 hours at room temperature, rinsed, dehydrated through an ethanol series and then infiltrated and embedded in methacrylate resin as described by Gubler (Gubler, 1989). 3 μm sections were attached to slides coated with Biobond (Electron Microscopy Sciences), incubated in acetone for 10 minutes to remove the resin, rehydrated, stained with Toluidine Blue O and examined with a 20× objective under bright field conditions in a Nikon Eclipse E600 microscope. Visualization of microtubules and F-actin in fixed cells was performed as described by Frank and Smith (Frank and Smith, 2002). For analysis of F-actin in living cells via transient expression of green-fluorescent-protein/talin (GFP-talin), strips of leaf tissue 2-8 cm from the bases of immature adult leaves 20-28 cm long were excised and cultured as described by Gallagher and Smith (Gallagher and Smith, 1999). Within 6 hours of the initiation of tissue cultures, plates were bombarded with 0.3-0.8 μg of pYSC14 (Kost et al., 1998) as described by Ivanchenko et al. (Ivanchenko et al., 2000), except that 1 μm gold particles were used as the microcarrrier, and tissue was cultured under continuous light conditions at 22°C for 22-26 hours prior to examining by confocal microscopy as described by Frank and Smith (Frank and Smith, 2002).

Double mutant analysis

To generate double mutants, homozygous *brk* mutants in a B73

background were crossed in each pairwise combination. F_1 progeny were selfed to generate an F_2 generation. Each mutant in the F_2 generation was test-crossed to both of the appropriate single mutants, and test-cross progeny were analyzed to determine the genotypes of the F_2 mutants. Cyanoacrylate glue impressions of leaf surfaces were examined under DIC conditions in a Nikon E600 microscope using a 10× objective, captured with a DAGE MTI CCD72 camera coupled to a Scion LG-3 framegrabber, and processed with Adobe Photoshop 4.0. To collect data for Table 1, at least four images from each impression were captured from randomly chosen locations.

Mosaic analysis

For mosaic analysis, *brk3 Oy1-700/brk3 oy1*$^+$, *brk2 vp5/brk2 Vp5*$^+$ and *brk1 lw2/brk1 Lw2*$^+$ plants were crossed to wild-type plants to generate seeds of the following genotypes: *brk1 lw2*/*Brk1*$^+$ *Lw2*$^+$ (*n*=3500), *brk2 vp5*/*Brk2*$^+$ *Vp5*$^+$ (*n*=1500), and *brk3 Oy1-700*/*Brk3 oy1*$^+$ (*n*=1750). This crossing scheme ensured that each *brk* mutant allele would always be linked *in cis* with the marker mutation in the doubly heterozygous progeny. Seeds were germinated, irradiated and grown as described previously (Walker and Smith, 2002). As discussed below, *vp5*-marked *brk2* sectors were also generated by means of *Ac/Ds*-induced chromosome breakage. Glue impressions of the leaf surface spanning the entire width of each sector were inspected for the *brk* phenotype. Sectors showing the *brk* phenotype were then fixed and processed for epidermal peels as described by Gallagher and Smith (Gallagher and Smith, 1999). Epidermal peels and hand-cut cross sections from these sectors were examined in a Nikon E600 microscope under epifluorescence conditions using a rhodamine filter set, and under DIC conditions. Images were acquired and processed as described earlier for double mutant analysis.

RESULTS

Three Brick genes are required for normal leaf epidermal cell morphogenesis

The wild-type maize leaf epidermis is composed of linear files of cells with diverse shapes. Pavement cells have marginal lobes, finger-like projections that interlock with those of neighboring cells (Fig. 1A). Interspersed within the pavement cells are stomatal complexes, which are composed of two guard cells flanked by two subsidiary cells; each complex of four cells is contained within a single cell file (Fig. 1A, black arrowheads). A screen for EMS-induced mutations affecting epidermal cell morphogenesis in the maize leaf identified nine recessive mutations with a phenotype similar to that of *brick1* (Gallagher and Smith, 2000; Frank and Smith, 2002). In all of these mutants, pavement cells lack marginal lobes (Fig. 1B). In addition, stomatal subsidiary cells occasionally invade neighboring cell files and have a variety of abnormal shapes (Fig. 1B, Fig. 3A,D,G, black asterisks). Complementation tests demonstrated that the nine new *brk1*-like mutations define two additional genes, *Brk2* and *Brk3*. In spite of the striking alterations observed at the cellular level, the overall morphology of *brk* mutant leaves and plants appears normal, although *brk* plants are approximately one-third shorter and reach maturity several days later than their wild-type siblings.

To determine whether *brk* mutations affect cell morphology in other leaf layers in addition to the epidermis, internal tissue layers were examined. As found previously for *brk1* (Frank and Smith, 2002), transverse sections revealed no differences in the sizes, shapes or organization of cells in internal tissue layers of *brk2* or *brk3* leaves compared with the wild type (Fig. 1C,D). Furthermore, direct examination of isolated mesophyll cells confirmed that their lobed shapes are normal in both *brk2* and *brk3* mutant leaves (data not shown). However, epidermal cells of *brk2* and *brk3* mutant leaves appear more rounded in cross section than those of wild-type leaves. This appears to be due mainly to a lack of outer epidermal cell wall material filling the crevices between adjacent epidermal cells in wild type leaves (Fig. 1C,D, arrows).

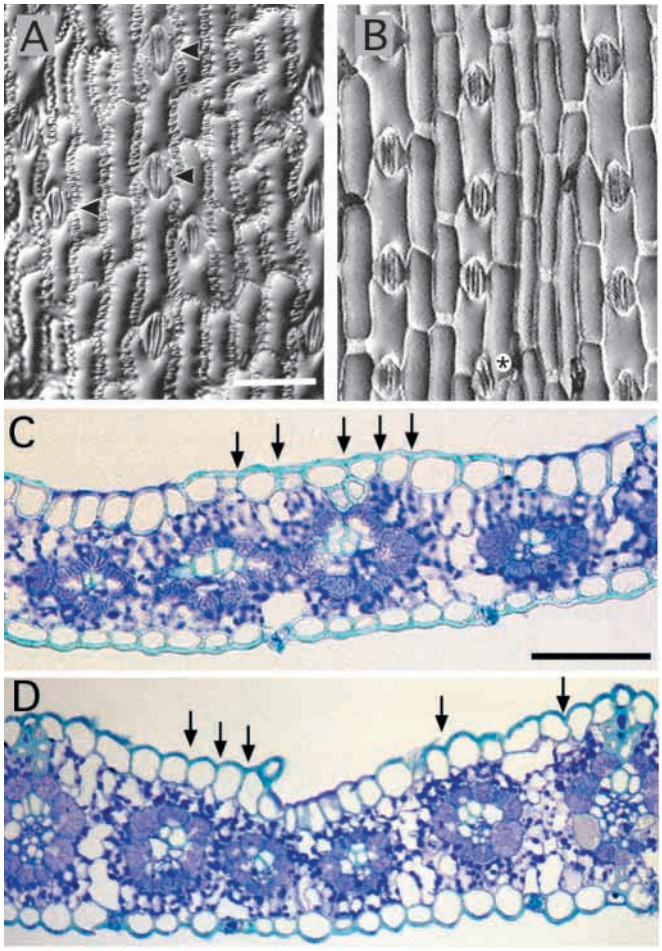

Fig. 1. Phenotypes of wild-type and *brk2* mutant leaves. Cyanoacrylate glue impressions of the abaxial surfaces of wild-type (A) and *brk2* (B) adult leaf blades. In A black arrowheads indicate stomata; in B black asterisk indicates an abnormal stomatal subsidiary cell. Toluidine-Blue-O-stained cross sections of wild-type (C) and *brk2* (D) adult leaf blades. Thickenings in the outer epidermal cell wall at the junctions between adjacent epidermal cells are seen in wild type but not *brk* mutant leaves (black arrows). In both epidermal impressions and cross sections, the *brk3* phenotype (not shown) is indistinguishable from that of *brk2*. Scale bars: 100 μm.

As discussed in the Introduction, several previous studies have attributed lobe formation in expanding epidermal and mesophyll cells to the organization of cortical microtubules into bands that direct a non-uniform pattern of cellulose deposition. As predicted from these earlier studies, cortical microtubules in expanding wild-type epidermal pavement cells of maize are organized into bands focused at lobe sinuses (Fig. 2A, white arrows). In expanding *brk1* pavement cells, cortical microtubules also form bands, although they are less distinct

than those in wild-type cells (Frank and Smith, 2002). Similarly, in expanding *brk2* and *brk3* pavement cells, cortical microtubule bands are observed that are less distinct than those in wild-type cells (Fig. 2B,C compared with 2A) but more pronounced than in those in *brk1* cells. Furthermore, cortical microtubules in expanding *brk2* and *brk3* pavement cells generally appear more aligned with each other than those in *brk1* or wild-type pavement cells (Fig. 2B,C compared with 2A) and are sometimes aligned at an oblique angle to the cell's long axis (Fig. 2C for *brk3*). Thus, as in *brk1* mutants, failure of pavement cell lobes to form in *brk2* and *brk3* mutants could not be readily explained in terms of a lack of cortical microtubule bands during cell expansion.

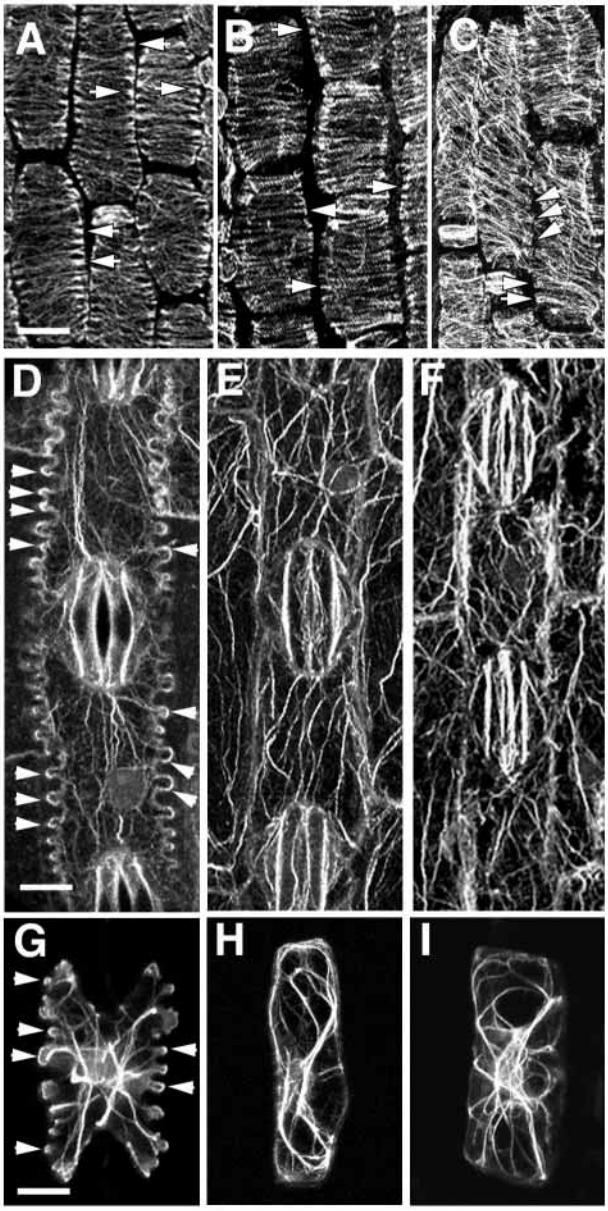

Fig. 2. Cytoskeletal organization in expanding epidermal pavement cells of wild-type, *brk2* and *brk3* maize leaves. (A) In wild-type cells, cortical microtubules form bands focused at lobe sinuses; these bands are also observed in *brk2* (B) and *brk3* (C) cells (arrows). In the wild type, FITC-phalloidin staining of fixed cells (D) and GFP-talin expression in living cells (G) reveal enrichments of cortical F-actin localized at lobe tips (arrowheads). Such cortical F-actin patches are not observed in *brk2* and *brk3* cells fixed and stained with FITC-phalloidin (E and F, respectively) or expressing GFP-talin (H and I, respectively). Scale bars: 13 μm.

Recent studies of actin organization in expanding epidermal pavement cells of wild-type maize and *Arabidopsis* revealed local accumulations of F-actin at the tips of emerging and elongating lobes (Fig. 2D, white arrows) (Frank and Smith, 2002; Fu et al., 2002). However, in *brk1* mutants, localized accumulations or 'patches' of cortical F-actin were not observed at any stage of pavement cell expansion (Frank and Smith, 2002). F-actin organization is similarly altered in *brk2* and *brk3* expanding pavement cells: no cortical F-actin patches were observed when fixed tissues were stained with FITC-phalloidin (Fig. 2E,F).

To confirm that these observations were not due to an artefact of chemical fixation, F-actin organization was also examined in living cells transiently expressing a GFP-talin fusion protein (Kost et al., 1998) introduced via particle bombardment. As in fixed, FITC-phalloidin-stained cells, expanding wild-type pavement cells expressing GFP-talin showed F-actin patches in elongating lobe tips (Fig. 2G, white arrows). In expanding *brk2* and *brk3* pavement cells expressing GFP-talin, no cortical F-actin patches were observed that were comparable to those seen in the wild type (Fig. 2H,I). Although small puncta of GFP-talin fluorescence were occasionally seen at the cell margins at early stages of mutant pavement cell expansion, they were not localized periodically and were generally restricted to small areas of the cell (data not shown). Thus, all three *Brk* genes are necessary for the formation of cortical F-actin patches, suggesting that they play an important role in pavement cell lobe formation.

The resemblance of F-actin organization at the tips of elongating pavement cell lobes to that in tip-growing cells led us to consider how *brk* mutations might affect cells known to expand by means of tip growth. No obvious alterations in the morphogenesis of root hairs were present in *brk2* or *brk3* mutants (data not shown). Moreover, when crosses are performed with *brk2* or *brk3* heterozygous pollen, mutant pollen tubes achieve fertilization at approximately the same frequency as competing wild-type pollen tubes. Thus, as in *brk1* (Frank and Smith, 2002), tip growth in *brk2* and *brk3* mutant root hairs and pollen tubes appears to be normal.

Brk1, *Brk2* and *Brk3* act in a common pathway

Double mutant analysis was used to investigate the relationships between the functions of *Brk1*, *Brk2* and *Brk3*. In populations segregating both single and double mutants derived from self-pollination of double heterozygotes, no phenotype distinct from the *brk* single mutant phenotype was observed. The genotype of each plant showing a mutant phenotype was determined by test-crossing to the appropriate single mutants. Pavement cell shapes in *brk1;brk2*, *brk2;brk3* and *brk1;brk3* double mutants are the same as those in *brk* single mutants (Fig. 3). The frequency of abnormal stomatal subsidiaries provides a more quantitative measure of phenotypic severity. In this respect, *brk1* (20-40% abnormal subsidiaries) is more severe than either *brk2* or *brk3* (5-10% abnormal subsidiaries; Table 1). Abnormal subsidiary frequencies in *brk1;brk3* and *brk1;brk2* double mutants are

similar to those in *brk1* single mutants, whereas abnormal subsidiary frequencies in *brk2;brk3* double mutants are similar to those in both *brk2* and *brk3* single mutants (Fig. 3; Table 1). Thus, all three classes of *brk* double mutants have the same phenotypes as *brk* single mutants, indicating that all three *Brk* genes function in a common pathway.

Construction and analysis of genetic mosaics

To gain a better understanding of the function of each *Brk* gene, clonal sectors of *brk* mutant cells in otherwise wild-type leaves were examined to determine whether each of the *Brk* genes acts cell-autonomously or non cell-autonomously. For any one of the *brk* mutations, if *brk* cells neighboring wild-type cells always show the mutant phenotype then that *Brk* gene acts cell-autonomously. However, if *brk* mutant cells next to wild-type cells show a wild-type phenotype then the corresponding gene acts non cell-autonomously.

Mosaic analysis of each *brk* mutation involved a similar scheme for generation of marked, clonal sectors, which is summarized in Fig. 4A. Seedlings heterozygous for a *brk* mutation linked *in cis* with a recessive or semi-dominant cell-autonomous marker mutation affecting chlorophyll pigmentation were irradiated to produce random chromosome breaks. Cells in which breaks have occurred between the centromere and the wild-type allele for the marker gene divide to produce white (albino) sectors of *brk* mutant cells in otherwise Brk^+, green plants. White sectors of *brk1*, *brk2* and *brk3* mutant tissue were analyzed to determine the locations of sector boundaries. Wild-type chloroplasts autofluoresce brightly when examined by fluorescence microscopy using a rhodamine filter set. Sector boundaries in internal tissue layers were located by examining leaf cross sections and in the epidermis by examining epidermal peels. In the epidermis, only stomatal guard cells contain mature chloroplasts and can therefore be scored as mutant or wild type for the albino mutation. Data collected through examination of cross sections and epidermal peels for each sector were compiled to reconstruct the composition of each sector (Fig. 4B).

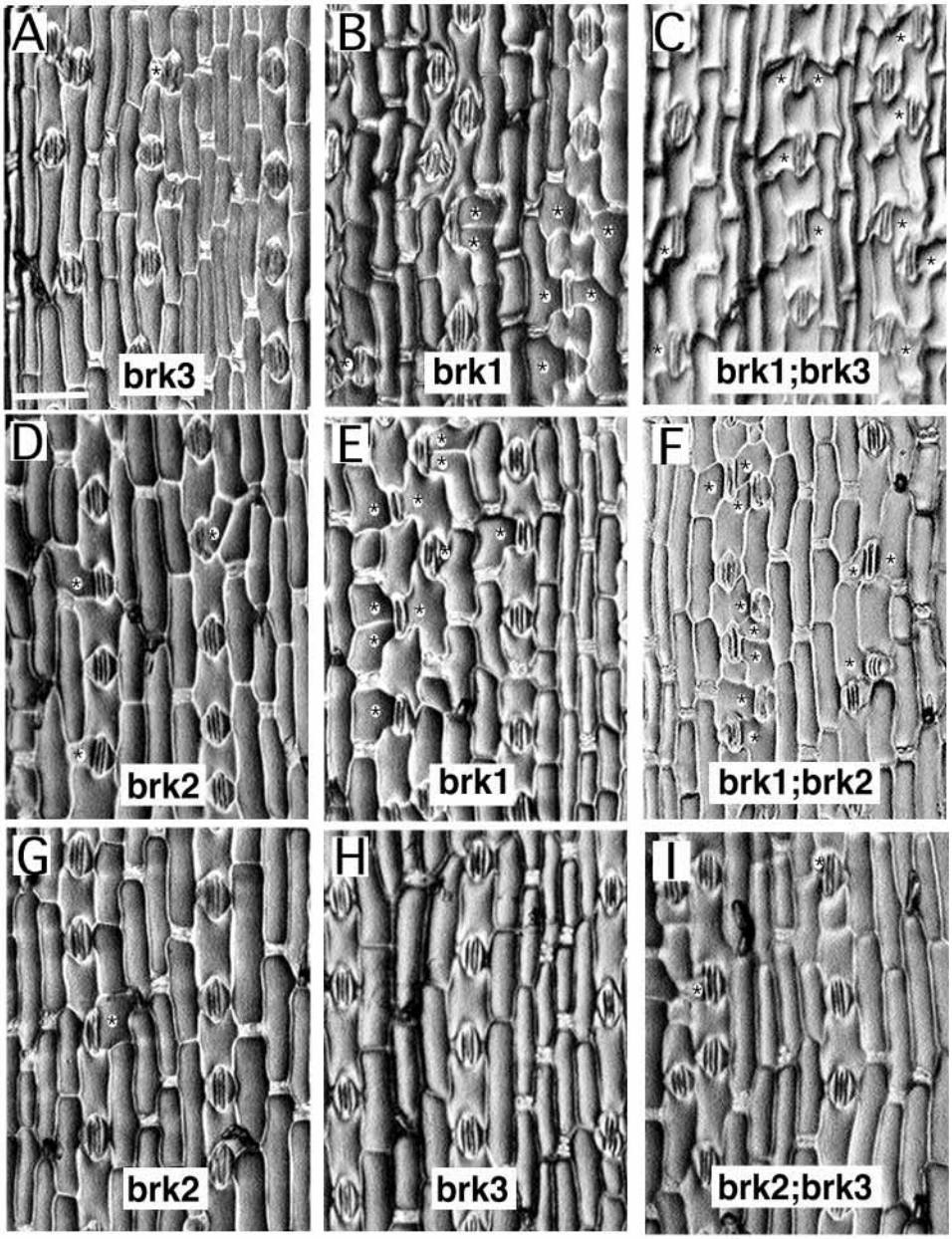

Fig. 3. Comparison of *brk* single and double mutant phenotypes. Glue impressions of adult leaf blades are shown for each double mutant and the corresponding single mutants from the same segregating population. (A-C) Single *brk3* (A), single *brk1* (B) and double *brk1;brk3* mutants (C). (D-F) Single *brk2* (D), single *brk1* (E) and double *brk1;brk3* mutants (F). (G-I) Single *brk2* (G), single *brk3* (H) and double *brk2;brk3* mutants (I). Asterisks indicate abnormal subsidiary cells. Scale bar: 100 μm.

Brk2 and *Brk3* act cell-autonomously to promote pavement cell lobe formation

Brk3 is located near the end of chromosome 10S, distal to the *Oil Yellow 1* (*Oy1*) locus (Fig. 4A). Plants heterozygous for the semi-dominant *Oy1-700* allele are yellow-green, whereas homozygous or hemizygous *Oy1-700* plants completely lack pigmentation and are therefore white. *Brk2* is located near the end of chromosome 1S ~6 cM from *Viviparous5* (*Vp5*). The *vp5* mutation is recessive; homozygous mutant plants are white. Albino-marked *brk2* and *brk3* sectors were generated by

Table 1. Analysis of abnormal subsidiary cells in *brk* single and double mutants

Genotype	Number of plants	Total number of stomata examined	Abnormal subsidiary cells (%)
brk1	4	807	27.8±8.7
brk2	5	943	9.0±3.7
brk3	3	642	4.8±0.5
brk1;brk3	4	1152	41.7±9.2
brk1;brk2	2	323	32.0
brk2; brk3	3	616	10.3±3.6

In each case, double mutants were compared with single mutants from the same segregating populations. Differences in the abnormal subsidiary frequencies in *brk1* single mutants vs. *brk1;brk3* double mutants, and in *brk2* single mutants vs. *brk2;brk3* double mutants, were found to be statistically insignificant, as determined by a Student's *t*-test (P>0.05).

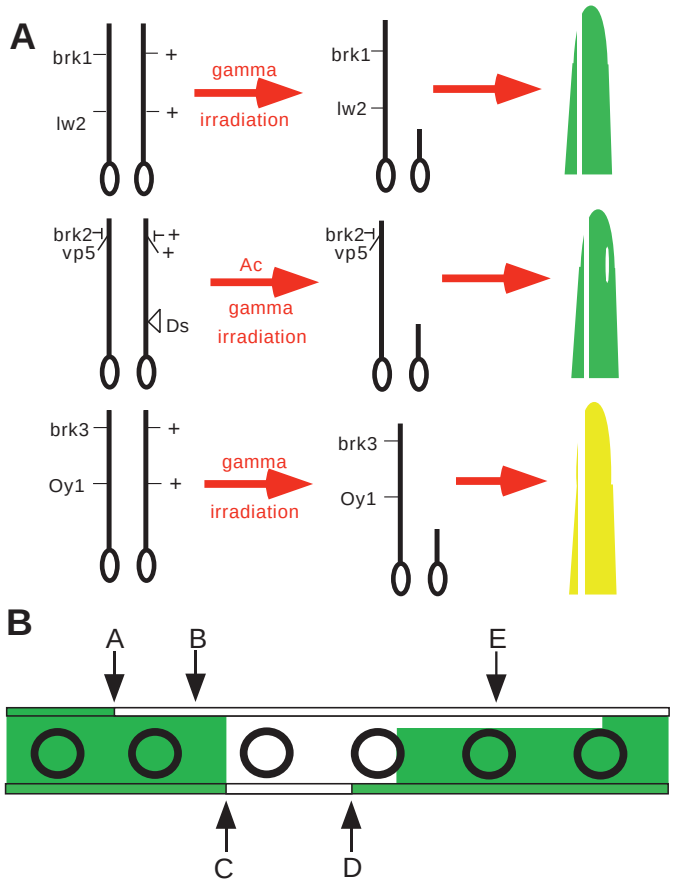

Fig. 4. Generation of marked *brk1*, *brk2* and *brk3* mutant sectors for mosaic analysis. (A) Relative locations of *brk* and marker loci are illustrated, along with the location of a chromosome-breaking *Ds* transposon used to generate marked *brk2* sectors. (B) Cross-sectional view of a hypothetical white sector in a green leaf illustrating all types of sector boundaries analyzed. Horizontal lines denote upper and lower epidermis; black circles denote veins. Green represents wild-type tissue; white represents mutant tissue. (A) Lateral boundary in the epidermis overlying wild type mesophyll. (B) Transverse boundary with mutant epidermis directly overlying wild-type mesophyll. (C) Lateral boundary in the epidermis coinciding with a lateral boundary in the mesophyll. (D) Lateral boundary in the epidermis overlying mutant mesophyll. (E) Transverse boundary having at least one layer of mutant mesophyll separating mutant epidermis from an underlying wild-type cell layer.

Table 2. Number of sector boundaries analyzed, classified as illustrated in Fig. 4A

Gene	Boundary type				
	A	B	C	D	E
brk1	21	28	14	28	47
brk2	42	30	11	19	20
brk3	31	37	19	14	20

Every sector with mutant epidermis overlying wild-type mesophyll has both type A and type B boundaries. Boundaries of type A, C and D were excluded from the analysis if they coincided with a major vein.

irradiating *brk3 Oy1-700* and *brk2 vp5* heterozygous plants (Fig. 4A) (described in Materials and Methods). A second method was also used to create *vp5*-marked *brk2* sectors. Plants homozygous for *brk2* and heterozygous for *vp5* were crossed to wild-type plants homozygous for a chromosome-breaking *Ds* transposon on chromosome 1S between the centromere and *Vp5* (Neuffer, 1995). In the progeny, *Ac*-induced chromosome breakage at the site of this *Ds* insertion resulted in the loss of wild-type *Vp5* and *Brk2* alleles, simultaneously uncovering *vp5* and *brk2*. Because *Ac/Ds*-induced chromosome breaks occur relatively late in development, the resulting sectors are small, sometimes only a few cell files in width, whereas sectors induced by irradiation are much larger (Fig. 4A).

We analyzed 72 *brk2* and 64 *brk3* lateral epidermal sector boundaries (Table 2; Fig. 4B, boundary types A, C and D). At all boundaries of this type, there was a clear difference between the shapes of *brk* and wild-type cells. As explained earlier, lateral sector boundaries in the epidermis can be located only to the interval between wild-type and albino stomatal files. Although stomatal files are usually separated by at least one non-stomatal file, we occasionally observed areas where sector boundaries split directly adjacent stomatal files such that one file was wild type and the neighboring file was mutant (Fig. 5A,B for *brk2*, Fig. 6A,B for *brk3*). In these areas, we could determine with certainty that wild-type cells were lobed, whereas directly adjacent *brk2* or *brk3* cells were unlobed. Glue impressions of lateral sector boundaries in the epidermis revealed that, at the junctions between wild-type and *brk2* or *brk3* pavement cells, lobes of wild-type cells appear to grow over unlobed, *brk* cells (Fig. 5C, black arrows, for *brk2*; Fig. 6C, black arrows, for *brk3*). These results demonstrate that both *Brk2* and *Brk3* act cell-autonomously in the lateral dimension to promote lobe formation in epidermal cells. We also analyzed transverse sector boundaries, where mutant epidermis lies over wild-type mesophyll (Fig. 4B, boundary type B). For *brk2* and *brk3*, respectively, 30 and 37 such boundaries were analyzed (Table 2). In each case, *brk* mutant epidermal cells overlying wild-type mesophyll cells were unlobed (Fig. 5A,B for *brk2*; Fig. 6A,B for *brk3*), indicating that *Brk2* and *Brk3* also act cell-autonomously in the transverse dimension.

Brk2 and *Brk3* act non cell-autonomously to promote polarized SMC divisions

In all *brk* mutants, stomatal subsidiaries occasionally form abnormally. Normal stomatal development in maize is illustrated in Fig. 7. An asymmetric division gives rise to a small guard mother cell (GMC), which is thought to signal its neighbors to the left and right (SMCs) to become polarized

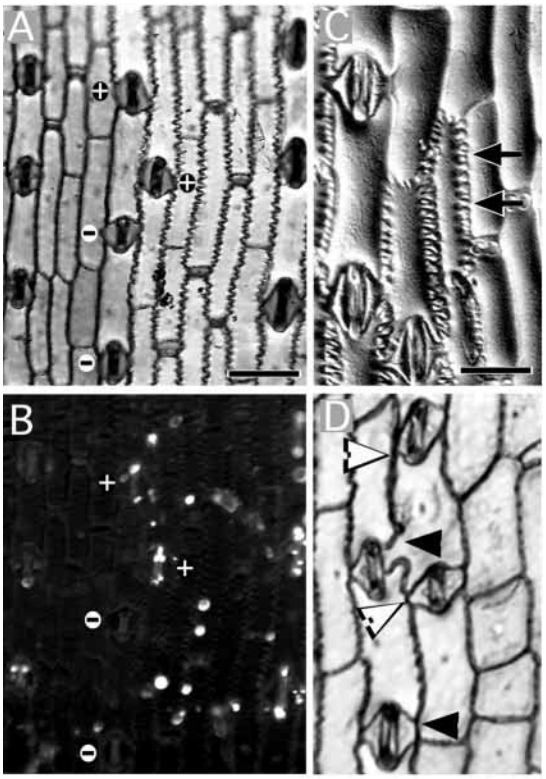

Fig. 5. Mosaic analysis of *brk2*. (A) DIC image of epidermal peel illustrating sector boundaries of types A and B (Fig. 4B). (B) Same field of view as in A but showing chlorophyll autofluorescence in wild-type guard cells. (A,B) White + signs indicate wild-type guard-cell pairs; black minuses indicate mutant guard-cell pairs in an adjacent cell file. Lobe formation in *brk2* mutant epidermal cells is not rescued by adjacent wild-type epidermal cells or underlying wild-type mesophyll. (C) DIC image of a glue impression showing junctions between *brk2* and wild-type pavement cells; black arrows indicate areas where the lobes of a wild-type cell appear to have grown over the top of an adjacent, unlobed mutant cell. (D) DIC image of an epidermal peel showing four mosaic stomata, two having a wild-type subsidiary flanking *brk2* mutant guard cells (white arrowheads), and two having a *brk2* mutant subsidiary flanking wild-type guard cells (black arrowheads); the upper one of these *brk2* subsidiary cells is abnormal. Scale bars: A, 100 μm; C, 50 μm.

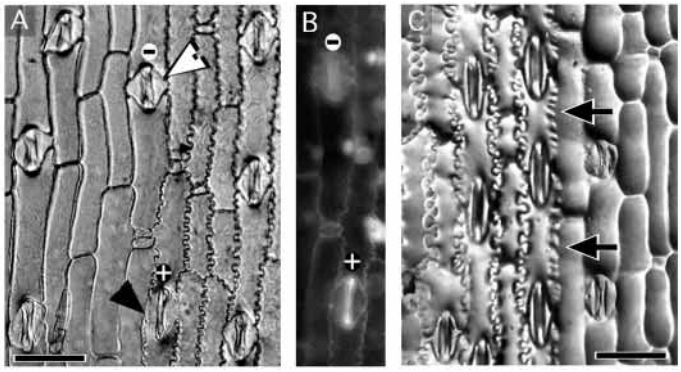

Fig. 6. Mosaic analysis of *brk3*. (A) DIC image illustrating sector boundaries of types A and B (see Fig. 4B). (B) Chlorophyll autofluorescence at same boundary shown in A. (A,B) A white plus sign indicates a wild-type guard-cell pair, which is flanked by a mutant subsidiary (black arrowhead in A); a black minus sign indicates a mutant guard-cell pair that is flanked by a wild-type subsidiary cell (white arrowhead in A). (C) DIC image of a glue impression showing junctions between *brk3* and wild-type pavement cells; black arrows indicate areas where the lobes of wild-type cells appear to have grown over the tops of adjacent, unlobed mutant cells. Scale bars: A, 100 μm; C, 70 μm.

Table 3. Proportion of abnormal subsidiary cells in *brk2* and *brk3* mosaic stomata at sector boundaries compared with fully mutant and fully wild-type stomata near sector boundaries

	Wild-type SMC + wild-type GMC	*brk* SMC + *brk* GMC	Wild-type SMC + *brk* GMC	*brk* SMC + wild-type GMC
brk2	3.3% (*n*=123)	18.4% (*n*=98)	3.3% (*n*=61)	10.5% (*n*=67)
brk3	0% (*n*=99)	15% (*n*=99)	0% (*n*=52)	1.5% (*n*=65)

GMC, guard mother cell; SMC, subsidiary mother cell.

with respect to the GMC and to divide asymmetrically to form subsidiary cells. The GMC later divides longitudinally to give rise to a guard cell pair. Analysis of stomatal development in *brk1* mutants showed that abnormal subsidiaries arise from SMCs that failed to polarize properly before dividing (Gallagher and Smith, 2000). The presumed role of GMCs in stimulating the polarization of adjacent SMCs raises the interesting question of whether SMC polarization depends on *Brk* gene function in the GMC or in the SMC itself. We addressed this question by examining mosaic stomata in which mutant guard cells were flanked by a wild-type subsidiary, or vice versa.

In contrast to its cell-autonomous action in promotion of pavement cell lobe formation, analysis of mosaic stomata showed that *Brk3* acts non cell-autonomously to promote polarized SMC divisions. Wild-type subsidiary cells in sectored leaves were never abnormal, whether flanking wild-type or *brk3* guard cells, demonstrating that the presence of a wild-type *Brk3* allele in the SMC alone is sufficient for its normal division. Whereas 15% of *brk3* subsidiaries flanking *brk3* guard cells were abnormal, only 1.5% of *brk3* subsidiaries flanking wild-type guard cells were abnormal (Table 3; Fig. 6A, arrowheads), demonstrating that wild-type GMCs rescued the abnormal divisions of adjacent, mutant SMCs. Notably, however, the abnormal divisions of *brk3* SMCs were not rescued by adjacent wild-type pavement cells (*n*=117), so the adjacent GMC appears to be the only cell that can supply *Brk3* function to a *brk3* mutant SMC.

Similar analysis of *brk2* mosaic stomata showed that *Brk2* acts partially non cell-autonomously to promote the polarized divisions of SMCs. As for *Brk3*, the presence of a wild-type *Brk2* allele in the SMC is sufficient for its normal division, because 3.3% of wild-type subsidiaries in sectored leaves were abnormal whether flanking wild-type or *brk2* guard cells. Whereas 18.4% of *brk2* subsidiaries flanking *brk2* guard cells were abnormal, 10.5% of *brk2* subsidiaries flanking wild-type guard cells were abnormal (Table 3; Fig. 5D, arrowheads). Thus, *brk2* SMC divisions were partially rescued by an adjacent, wild-type GMC.

Brk1 acts non cell-autonomously

Brk1 is located near the end of chromosome 5S. As illustrated

in Fig. 4A, the recessive *lemon white 2* (*lw2*) mutation, located between the centromere and *brk1*, was used to mark *brk1* mutant sectors. To determine whether *Brk1* acts cell-autonomously or non cell-autonomously within the epidermis, we analyzed 63 lateral sector boundaries (Fig. 4B, types A, C and D). In areas where these boundaries split adjacent stomatal cell files, *brk1* cells in direct contact with wild-type cells appeared to be wild type, with pavement cell lobes and normal stomata (Fig. 8A,B). Moreover, weakly lobed pavement cells were observed in *brk1* mutant cells two to three cell files away from the nearest wild-type epidermal cell (Fig. 8A, black arrows). Thus, direct contact with a wild-type cell is not necessary to rescue the phenotype of a *brk1* cell. From these observations, we conclude that *Brk1* acts non cell-autonomously in the lateral dimension.

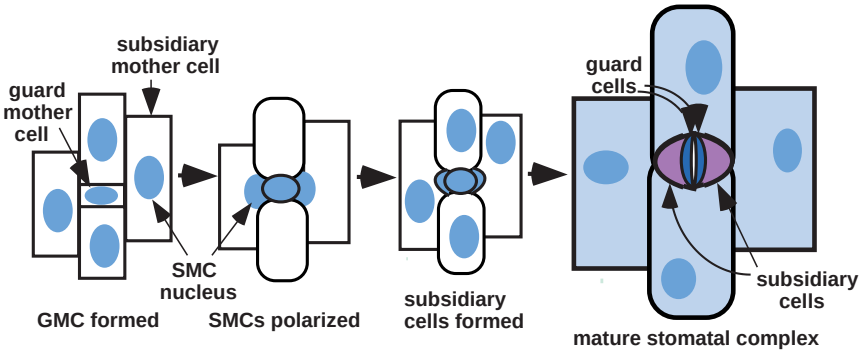

Fig. 7. Summary of stomatal development in maize (after Stebbins and Shah, 1960). Subsidiary mother cells flanking a guard mother cell become polarized and then divide asymmetrically to form stomatal subsidiary cells.

To investigate whether *Brk1* also acts non cell-autonomously in the transverse dimension, 53 sectors were identified in which *brk1* mutant epidermis was overlying wild-type internal tissue layers. At 28 boundaries with wild-type mesophyll directly underlying *brk1* epidermis (Fig. 4B, boundary type B), the mutant epidermis was indistinguishable from wild-type epidermis, with lobed pavement cells and normal stomata (Fig. 8C,D, right-hand side). By contrast, at 25 boundaries where *brk1* epidermis was separated from a wild-type cell layer by one or more layers of *brk1* mesophyll (Fig. 4B, boundary type E), the epidermis appeared to be mutant, lacking marginal lobes and having some abnormal subsidiary cells. These results show that *Brk1* is expressed and functions in internal tissue layers even though no mutant phenotype was observed in these layers of *brk1* leaves. Furthermore, *Brk1* expressed in these layers rescues the phenotype of directly overlying *brk1* mutant epidermal cells. Therefore, *Brk1* acts non cell-autonomously in the transverse dimension but its influence does not travel as far in this dimension as it does within the epidermis.

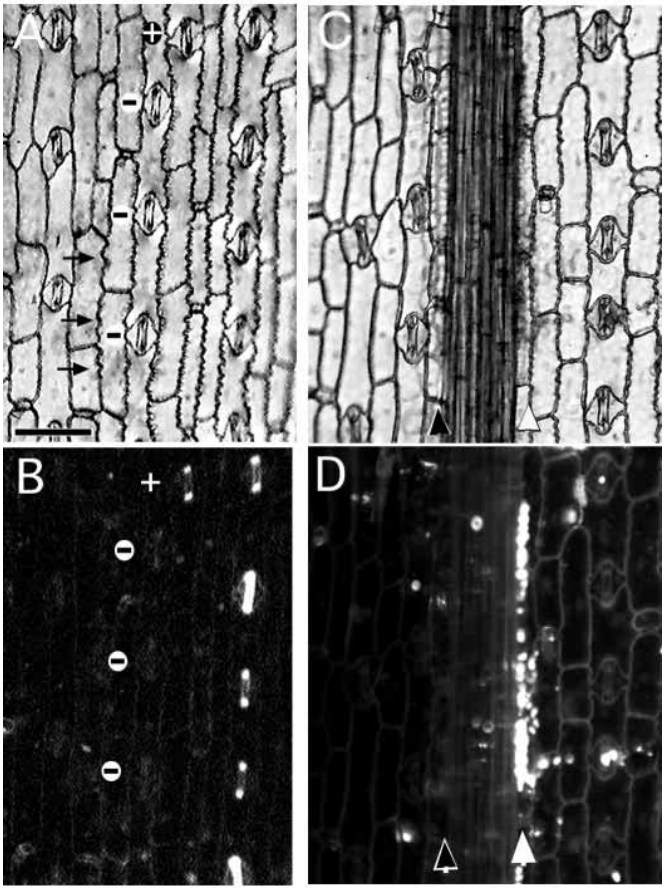

Fig. 8. Mosaic analysis of *brk1*. (A) DIC image of an epidermal peel illustrating a type D lateral sector boundary (Fig. 4B), which overlies *brk1* mesophyll. Scale bar: 110 μm. (B) Chlorophyll autofluorescence in same field of view shown in A. (A,B) A white plus sign indicates a wild-type stoma; black minus signs indicate *brk1* mutant stomata in files with lobed pavement cells. Arrows (A) indicate mutant pavement cells with weak marginal lobes that are separated from wild-type cells by one file of mutant cells. (C) DIC image of an epidermal peel illustrating a type B transverse sector boundary (see Fig. 4B). (D) Chlorophyll autofluorescence in same field as shown in C. Epidermal cells with a *brk1* mutation appear mutant where they overlie *brk1* mesophyll (left of black arrowhead) but wild type where they directly overlie wild-type mesophyll (right of white arrowhead).

DISCUSSION

In this study, we have used a variety of genetic approaches to analyze the functions of three *Brk* genes involved in epidermal cell morphogenesis and division in the maize leaf. All three *Brk* genes are required for the formation of polarized outgrowths giving rise to lobes on the margins of epidermal pavement cells but not for cell expansion in general, and are also involved in the polarized divisions of SMCs.

Consistent with many previous studies of lobe formation, cortical microtubules are organized into bands focused at lobe sinuses of expanding wild-type pavement cells in the maize leaf epidermis. In spite of the absence of lobe formation, these microtubule bands are also present in all three *brk* mutants, although they are somewhat less distinct. Visualization of F-actin in expanding wild-type pavement cells by means of phalloidin staining of fixed cells and GFP-talin expression in living cells showed distinct enrichments of cortical F-actin at lobe tips. These observations are similar to those reported in a recent study in which F-actin organization was visualized in

living, expanding *Arabidopsis* epidermal pavement cells expressing GFP-talin (Fu et al., 2002). Another recent study of lobe formation in *Arabidopsis* pavement cells revealed relatively little enrichment of cortical F-actin in lobe tips (Qiu et al., 2002). In this study, however, antibody staining of fixed cells was used to visualize F-actin, so some cortical F-actin might have been lost during the fixation process. Our observation of cortical F-actin enrichments at lobe tips in both fixed and living maize cells indicates that this feature of cytoskeletal organization is not an artefact of the F-actin visualization method used. In both living and fixed expanding epidermal pavement cells of all three *brk* mutants, cortical F-actin enrichments were not observed, supporting the conclusion that these F-actin enrichments are important for lobe formation, and indicating that the *Brk* genes are required for their formation. By analogy to the proposed function of F-actin in both tip-growing and diffusely growing cells, the F-actin enriched in lobe tips might function to guide or promote localized secretion.

Analysis of *brk1;brk2*, *brk1;brk3* and *brk2;brk3* double mutants showed that they have the same phenotypes as the corresponding single mutants. These results indicate that all three *Brk* genes act in a common pathway. Although this might mean that the genes act in a linear sequence, it is also possible that the products of these genes simply act together in a common process, possibly directly interacting with each other. Although the *Brk1* gene product has been identified (Frank and Smith, 2002), investigation of its functional relationship to *Brk2* and *Brk3* gene products awaits the cloning of these other two genes.

Mosaic analyses were carried out to determine whether each *Brk* gene acts cell-autonomously or non cell-autonomously. *Brk1* acts non cell-autonomously in both lateral and transverse leaf dimensions over a short distance. Although the non cell-autonomous influence of *Brk1* does not depend on direct cell-cell contact, it travels farther within the epidermal layer (2-3 cell diameters) than it does between leaf layers (1 cell diameter). The non cell-autonomous action of *Brk1* suggests that this gene encodes or controls the production of a diffusible or transported molecule. The *Brk1* gene was shown to encode a novel protein of ~8 kDa that is highly conserved in both plants and animals (Frank and Smith, 2002). Neither BRK1 nor BRK1-related proteins in other organisms have the predicted signal peptides expected for secreted proteins. Moreover, recent work has implicated the mammalian BRK1 homolog HSPC300 in the regulation of actin polymerization (Eden et al., 2002), clearly pointing to an intracellular function for BRK1. However, the non cell-autonomous action of *Brk1* might reflect movement of BRK1 from cell to cell through plasmodesmata. Particularly at early developmental stages, a variety of proteins considerably larger than BRK1 appear to be transported from cell to cell via plasmodesmata in maize and several other plant species (Jackson, 2000). Whether the BRK1 protein moves intercellularly and the functional significance of any such movement remain to be determined.

Unlike *Brk1*, mosaic analyses showed that *Brk2* and *Brk3* act cell-autonomously to promote the formation of epidermal pavement cell lobes, indicating that both gene products act in or on each pavement cell to direct its own morphogenesis. Surprisingly, however, *Brk3* acts non cell-autonomously, and *Brk2* partially non cell-autonomously, to promote the polarized divisions of SMCs. Although polarization of SMCs appears to depend on a signal from the adjacent guard mother cell (GMC), it is unlikely that *Brk3* or *Brk2* function directly in this signaling process. If they did, we would expect that a subsidiary cell's phenotype would depend solely on the genotype of its adjacent GMC, but we found instead that the presence of a wild-type *Brk3* allele in either the SMC or the adjacent GMC is sufficient for a normal SMC division. The same is true for *Brk2*, except that a wild-type *Brk2* allele in the GMC only partially rescues the polarized divisions of adjacent *brk2* SMCs. In summary, the *Brk2* and *Brk3* function needed for polarized SMC divisions can be provided by the SMC itself, or by the adjacent GMC, but not by surrounding pavement cells. The specificity observed in the non cell-autonomous action of *Brk3* and *Brk2* might be due to diffusion or active transport of BRK3 protein (and to a lesser extent, BRK2 protein) from GMCs to SMCs, but not between other leaf cell types. Alternatively, presence of BRK3 and BRK2 proteins in either the SMC or the GMC might in some way facilitate intercellular communication between these two cell types leading to proper polarization of SMCs.

In summary, genetic and phenotypic analyses of *brk* mutations show that they define three genes that act in a common pathway promoting specific aspects of maize leaf epidermal morphogenesis and division that involve local actin polymerization. Moreover, mosaic analyses yielding different results for each *Brk* gene show that the product of each gene has a distinct function in that pathway. The mammalian homolog of BRK1, HSPC300, has recently been directly implicated in regulation of Arp2/3-dependent actin polymerization (Eden et al., 2002). The Arp2/3 complex (putative components of which are encoded by various plant genomes) nucleates polymerization of new actin filaments at specific sites in the cell when activated by proteins that respond to localized intracellular or extracellular cues (Higgs and Pollard, 2001). HSPC300 was identified as a component of a multiprotein complex isolated from bovine brain extracts that also includes WAVE, an Arp2/3 activator whose activity is regulated by Rac. The intact WAVE complex is inactive but, in the presence of GTP-Rac (or Nck, another regulatory protein), WAVE and HSPC300 dissociate from the rest of the complex to form a two-protein subcomplex that stimulates Arp2/3-dependent actin polymerization (Eden et al., 2002). Thus, BRK1 probably functions as part of a complex that also contains an Arp2/3 activator. *Brk2* and *Brk3* might encode other components of such a BRK1-containing complex, or factors that positively regulate its activity. Indeed, either *Brk2* or *Brk3* might encode a WAVE ortholog, a particularly exciting possibility given that plant genomes are not predicted by sequence homology to encode WAVE-like proteins or other Arp2/3 activators. Interestingly, the *Arabidopsis SPK1* gene is also required for the formation of epidermal pavement cell lobes; this encodes a protein containing a motif that has previously been shown to interact with Rac GTPases (Qiu et al., 2002). Moreover, expression of both dominant negative and constitutively active forms of the Rac/Rho-related *Arabidopsis* GTPase ROP2 also perturbs the formation of epidermal pavement cell lobes (Fu et al., 2002). In combination with recent findings on the role of HSPC300 in regulation of local actin polymerization by Rac, these findings suggest that BRK

proteins might function in the same pathway (probably downstream of) maize SPK1 and ROP2 orthologs. To investigate these possibilities, future work will be aimed at the identification and analysis of *Brk2* and *Brk3* gene products.

We thank Challe Woosley, Dan Burnes, Miroslav Dudas and Andy Teng for their contributions to this work. We also thank Lisa Harper and Michael Freeling for F_2 populations segregating EMS-induced mutations, Gerry Neuffer for chromosome-breaking *Ds* insertion lines, Phil Becraft for the *Oy1-700* allele and advice for its use as a marker for mosaic analysis, the Maize Genetics Coop. for seeds and RFLP markers, Nam-Hai Chua for the pYSC14 GFP-talin plasmid, the Torrey Mesa Research Institute for use of their particle gun, and Shiping Zhang for his help with use of the gun. Thanks also to Adrienne Roeder, Anne Sylvester, David Jackson and members of the Smith lab for helpful discussions. This work was supported by NSF grant IBN-9817084 to L.G.S.

REFERENCES

Apostolakos, P., Galatis, B. and Panteris, E. (1991). Microtubules in cell morphogenesis and intercellular space formation in *Zea mays* leaf mesophyll and *Pilea cadierei* epithem. *J. Plant Physiol.* **137**, 591-601.

Baskin, T. I. (2001). On the alignment of cellulose microfibrils by cortical microtubules: a review and a model. *Protoplasma* **215**, 150-171.

Baskin, T. I. and Bivens, N. J. (1995). Stimulation of radial expansion in *Arabidopsis* roots by inhibitors of actomyosin and vesicle secretion but not by various inhibitors of metabolism. *Planta* **197**, 514-521.

Beckett, J. B. (1994). Locating recessive genes to chromosome arm with B-A translocations. In *The Maize Handbook* (ed. M. Freeling and V. Walbot), pp. 315-327. New York: Springer-Verlag.

Bouyer, D., Kirik, V. and Hulskamp, M. (2001). Cell polarity in *Arabidopsis* trichomes. *Semin. Cell Dev. Biol.* **12**, 353-356.

Burk, D. H., Liu, B., Zhong, R., Morrison, W. H. and Ye, Z. H. (2001). A katanin-like protein regulates normal cell wall biosynthesis and cell elongation. *Plant Cell* **13**, 807-827.

Cyr, R. J. (1994). Microtubules in plant morphogenesis: role of the cortical array. *Annu. Rev. Cell Biol.* **10**, 153-180.

Dong, C.-H., Xia, G.-X., Hong, Y., Ramachandran, S., Kost, B. and Chua, N.-H. (2001). ADF proteins are involved in the control of flowering and regulate F-actin organization, cell expansion, and organ growth in *Arabidopsis*. *Plant Cell* **13**, 1333-1346.

Eden, S., Rohtagi, R., Podtelejnikov, A. V., Mann, M. and Kirschner, M. W. (2002). Mechanism of regulation of WAVE1-induced actin nucleation by Rac1 and Nck. *Nature* **418**, 790-793.

Folkers, U., Kirik, V., Schobinger, U., Falk, S., Krishnakumar, S., Pollock, M. A., Oppenheimer, D. G., Day, I., Reddy, A. R., Jürgens, G. et al. (2002). The cell morphogenesis gene *ANGUSTIFOLIA* encodes a CtBP/BARS-like protein and is involved in the control of the microtubule cytoskeleton. *EMBO J.* **21**, 1280-1288.

Frank, M. J. and Smith, L. G. (2002). A small, novel protein highly conserved in plants and animals promotes the polarized growth and division of maize leaf epidermal cells. *Curr. Biol.* **12**, 849-853.

Fu, Y., Li, H. and Yang, Z. (2002). The ROP2 GTPase controls the formation of cortical fine F-actin and the early phase of directional cell expansion during *Arabidopsis* organogenesis. *Plant Cell* **14**, 777-794.

Gallagher, K and Smith, L. G. (1999). *discordia* mutations specifically misorient asymmetric cell divisions during development of the maize leaf epidermis. *Development* **126**, 4623-4633.

Gallagher, K. and Smith, L. G. (2000). Roles for polarity and nuclear determinants in specifying daughter cell fates after an asymmetric division in the maize leaf. *Curr. Biol.* **10**, 1229-1232.

Geitmann, A. and Emons, A. M. C. (2000). The cytoskeleton in plant and fungal cell tip growth. *J. Microsc.* **198**, 218-245.

Giddings, T. H., Jr and Staehelin, L. A. (1991). Microtubule-mediated control of microfibril deposition: a re-examination of the hypothesis. In *The Cytoskeletal Basis of Plant Growth and Form* (ed. C. W. Lloyd), pp. 85-99. London: Academic Press.

Gubler, F. (1989). Immunofluorescence localization of microtubules in plant root tips embedded in butyl-methyl methacrylate. *Cell Biol. Int. Rep.* **13**, 137-146.

Hepler, P. K., Vidali, L. and Cheung, A. Y. (2001). Polarized cell growth in higher plants. *Annu. Rev. Cell Dev. Biol.* **17**, 159-187.

Higgs, H. N. and Pollard, T. D. (2001). Regulation of actin filament network formation through ARP2/3 complex: activation by a diverse array of proteins. *Annu. Rev. Biochem.* **70**, 649-676.

Ivachenko, M., Vejlupkova, Z., Quatrano, R. S. and Fowler, J. E. (2000). Maize ROP7 GTPase contains a unique, CaaX box-independent plasma membrane targeting signal. *Plant J.* **24**, 79-90.

Jackson, D. (2000). Opening up the communication channels: recent insights into plasmodesmal function. *Curr. Opin. Plant Biol.* **3**, 394-399.

Jung, G. and Wernicke, W. (1990). Cell shaping and microtubules in developing mesophyll of wheat (*Triticum aestivum* L.). *Protoplasma* **153**, 141-148.

Kim, G.-T., Shoda, K., Tsuge, T., Cho, K.-H., Uchimiya, H., Yokoyama, R., Nishitani, K. and Tsukaya, H. (2002). The *ANGUSTIFOLIA* gene of *Arabidopsis*, a plant CtBP gene, regulates leaf-cell expansion, the arrangement of cortical microtubules in leaf cells and expression of a gene involved in cell-wall formation. *EMBO J.* **21**, 1267-1279.

Kost, B., Spielhofer, P. and Chua, N.-H. (1998). A GFP-mouse talin fusion protein labels plant actin filaments in vivo and visualizes the actin cytoskeleton in growing pollen tubes. *Plant J.* **16**, 393-401.

Mathur, J., Spielhofer, P., Kost, B. and Chua, N.-H. (1999). The actin cytoskeleton is required to elaborate and maintain spatial patterning during trichome cell morphogenesis in *Arabidopsis thaliana*. *Development* **126**, 5559-5568.

Neuffer, M. G. (1995). Chromosome breaking sites for genetic analysis in maize. *Maydica* **40**, 99-116.

Oppenheimer, D. G., Pollock, M. A., Vacik, J., Szymanski, D. B., Ericson, B., Feldmann, K. and Marks, M. D. (1997). Essential role of a kinesin-like protein in *Arabidopsis* trichome morphogenesis. *Proc. Natl. Acad. Sci USA* **94**, 6261-6266.

Panteris, E., Apostolakos, P. and Galatis, B. (1993a). Microtubule organization, mesophyll cell morphogenesis, and intercellular space formation in *Adiantum capillus veneris* leaflets. *Protoplasma* **172**, 97-110.

Panteris, E., Apostolakos, P. and Galatis, B. (1993b). Microtubules and morphogenesis in ordinary epidermal cells of *Vigna sinensis* leaves. *Protoplasma* **174**, 91-100.

Panteris, E., Apostolakos, P. and Galatis, B. (1994). Sinuous ordinary epidermal cells: behind several patterns of waviness, a common morphogenetic mechanism. *New Phytol.* **127**, 771-780.

Qiu, J.-L., Jilk, R., Marks, M. D. and Szymanski, D. B. (2002). The *Arabidopsis SPIKE1* gene is required for normal cell shape control and tissue development. *Plant Cell* **14**, 101-118.

Smith, L. G. (2003). Cytoskeletal control of plant cell shape: getting the fine points. *Curr. Opin. Plant Biol*. (in press).

Stebbins, G. L. and Shah, S. S. (1960). Developmental studies of cell differentiation in the epidermis of monocotyledons. II. Cytological features of stomatal development in the *Gramineae*. *Dev. Biol.* **2**, 477-500.

Szymanski, D. B., Marks, M. D. and Wick, S. M. (1999). Organized F-actin is essential for normal trichome morphogenesis in *Arabidopsis*. *Plant Cell* **11**, 2331-2347.

Walker, K., and Smith, L. G. (2002). Investigation of the role of cell-cell interactions in division plane determination during maize leaf development through mosaic analysis of the *tangled* mutation. *Development* **129**, 3219-3226.

Wasteneys, G. O., Willingdale-Theune, J. and Menzel, D. (1997). Freeze shattering: a simple and effective method for permeabilizing higher plant cell walls. *J. Microsc.* **188**, 51-61.

Wernicke, W. and Jung, G. (1992). Role of cytoskeleton in cell shaping of developing mesophyll of wheat (*Triticum aestivum* L.). *Eur. J. Cell Biol.* **57**, 88-94.

Wernicke, W., Gunther, P. and Jung, G. (1993). Microtubules and cell shaping in the mesophyll of *Nigella damascena* L. *Protoplasma* **173**, 8-12.